coatings

MDPI

*Article*

# Microstructure and Wear Resistance of Fe60 Laser Cladding Coating Assisted by Steady Magnetic Field–Mechanical Vibration Coupling Field

**Yueyi Wang †, Hai Shi †, Xuanhong Hao, Hongxi Liu * and Xiaowei Zhang ***

The Faculty of Materials Science and Engineering, Kunming University of Science and Technology, Kunming 650093, China; wangyueyi@stu.kust.edu.cn (Y.W.); sayhay@yeah.net (H.S.); hxh_instinct@163.com (X.H.)

* Correspondence: piiiliuhx@sina.com (H.L.); zhxw72@163.com (X.Z.)

† These authors contributed equally to this work.

**Abstract:** Fe60 laser cladding coating was prepared on the surface of 45 steel with the assistance of alternating magnetic field–mechanical vibration coupling field. The XRD results show that the coating is mainly composed of solid solution Ni-Cr-Fe, (Fe, Ni), and Fe-Cr and also contains a certain amount of Cr2Fe14C hard phase. In the process of laser cladding, the chemical composition of the coating is not affected by the coupling field. Under the interaction of the coupling field, the liquid metal in the molten pool is fully stirred; the heat diffusion in the molten pool is accelerated; the temperature gradient in front of the solid–liquid interface decreases; and the large-size dendrites are broken. Those contribute to the grains being refined significantly in the coating. In addition, the content of Cr2Fe14C hard phase in the coating is increased under the coupling field. The maximum microhardness of the coating can reach 702 $HV_{0.2}$, and the corrosion rate of the coating is the lowest under the coupling field, while the weight loss of the 45 steel surface with the action of the coupling field is 68.9% lower than that without coupling field. The laser cladding technology assisted by alternating magnetic field–mechanical vibration coupling field can promote the development of a wear-resistant coating field.

**Keywords:** laser cladding; alternating magnetic field–mechanical vibration coupling field; Fe60 coating; microstructure; wear resistance



**Citation:** Wang, Y.; Shi, H.; Hao, X.; Liu, H.; Zhang, X. Microstructure and Wear Resistance of Fe60 Laser Cladding Coating Assisted by Steady Magnetic Field–Mechanical Vibration Coupling Field. *Coatings* **2022**, *12*, 751. https://doi.org/10.3390/coatings12060751

Academic Editor: Alina Vladescu

Received: 6 April 2022
Accepted: 16 May 2022
Published: 31 May 2022



## 1. Introduction

Laser cladding is an effective technology for improving strength, hardness, wear resistance, and other surface properties of materials [1–3]. However, the melting and solidification of alloy powder and substrate are quickly completed during the process of laser cladding, and the difference in the chemical composition of alloy powder and substrate leads to the unsatisfactory properties of the cladding layer, such as high porosity, cracking, and composition dilution [4–6]. These matters seriously restrict the preparation of high-quality laser cladding layers.

To improve the quality of the laser cladding layers, the researchers attempt to introduce an external energy field into the process of laser cladding (for example, magnetic field and vibration field) [4,7–9]. Much research proves that the external vibration field can provide excitation force for the molten pool which breaks and refines the primary crystal in the molten pool crystallization process and provides more nucleation particles for the unsolidified metal liquid. Importantly, the effect on the microstructure, such as grain shape and size, dendrite growth direction, and precipitation, can be achieved. Therefore, the microstructure and performance of the coating are improved apparently [7,10–13]. In addition, the hard phase can be formed by the combination of carbon and Cr or other elements in the iron-based alloy powder during the process of laser cladding, and, thus,

the wear resistance of the coating is enhanced [14,15]. Some works show that the grains are refined and that the depth of the molten pool is controlled by the laser surface treatment which is assisted by the ultrasonic vibration field [16,17]. In addition, the magnetic field is also an effective external energy field which contributes to the improvement of the quality of laser cladding layers in the research of laser cladding assisted by the electromagnetic field, which contains three forms: single electric field, single magnetic field, and electromagnetic composite field. The effects of a single magnetic field-assisted laser cladding layer can be divided into a steady magnetic field and alternating/rotating magnetic field [18]. Lorentz force can be generated in the molten pool under the influence of electric field and magnetic field. The Lorentz force in the steady magnetic field is the resistance to convection in the molten pool, which can restrain ripples on the molten pool surface [19,20]. In order to make up for the deficiency of a single field-assisted laser cladding, the coating structure can be optimized by a coupled field-assisted laser cladding. One way is with the laser cladding assisted by coupled field with electric and magnetic [18,21]. In addition, the laser cladding assisted by coupled field with mechanical vibration and alternating magnetic is also an efficient approach; some research has shown that the dendrites are broken and the free growth of dendrites is hindered by the vibration field, which reduces the size of the grains. Meanwhile, the pinch effect generated by the magnetic field can also further refine the grains. Therefore, the mechanical properties of the alloy are improved [22–24]. In addition, the inhibition of the solute diffusion and the decrease of the component dilution rates can be achieved by a steady magnetic field [18,25]. However, there are few reports on the laser cladding assisted by coupled field with mechanical vibration and magnetic.

Based on this, the laser cladding coating assisted by the coupled field with vibration and steady magnetic was investigated in this work. According to the characteristics of crystal growth during solidification and crystallization of laser cladding pool, a coupled fields device that integrated the advantages of mechanical vibration and the magnetic field is designed. With this device, Fe60 alloy coating was prepared on the surface of 45 steel by coupled field-assisted laser cladding. The structure, composition, and friction resistance of the coating were analyzed. Finally, the mechanism of the effect of grains in laser cladding coating caused by different field-assisted types was explained.

## 2. Experiment

### *2.1. Materials and Methods*

The 45 steel (Zhongxie Metal Materials Co., Ltd., Dongguan, China) with dimensions of 10 mm × 100 mm × 10 mm was worked as the substrates. The substrates were cleaned by ultrasonic wave with acetone and anhydrous alcohol to remove oil stains on the surface. The cladding material is Fe60 powder with a 60–150 mesh particle size (Jinnuo Welding Materials Co., Ltd., Nanjing, China), and the element content of the 45 steel and Fe60 powder are shown in Table 1. The schematic diagram of laser cladding experimental equipment is shown in Figure 1. The laser source was generated by the Gs-TFL-6000 cross-flow multi-mode $CO_2$ laser (Gs-TFL-6000, Golden sky laser system Co., Ltd., Wuhan, China). The mechanical field is generated by an electromagnetic vertical vibrator (Gaoxiang Machinery Equipment Co., Ltd., Dongguan, China). The magnetic field generating device is a self-made device, as shown in Figure S1. During the laser cladding process, the laser power was 4 kW; the defocusing ability was 25 mm; the spot diameter was 3 mm; and the scanning speed was 400 mm/min. The parameters of assisted field during the laser cladding are shown in Table 2, the sample of 1# represented the laser cladding which was not applied with assisted field. The sample of 2# indicated that the assisted vibration field with an amplitude of 3 mm and the vibration frequency of 100 Hz was applied during the laser cladding process. The sample of 3# was assisted by a magnetic field with 0.8 T. The sample of 4# was the sample that was assisted by coupled field with a vibration field (3 mm) and magnetic field (0.8 T). During the experiment, nitrogen was selected as the protective gas (purity 99.99%), and the gas flow was 15 L/h.

**Table 1.** The element content of 45 steel and Fe60 powder.

| Composition/wt.% | C | Si | Ni | W | B | Cr | Fe |
|---|---|---|---|---|---|---|---|
| 45 Steel | 0.43 | 0.17 | 0.30 | 0 | 0 | 0 | 98.35 |
| Fe60 | 4.0–4.5 | 2–3 | 4 to 6 | 2–3 | 1.5–2.5 | 24 to 30 | Bal. |

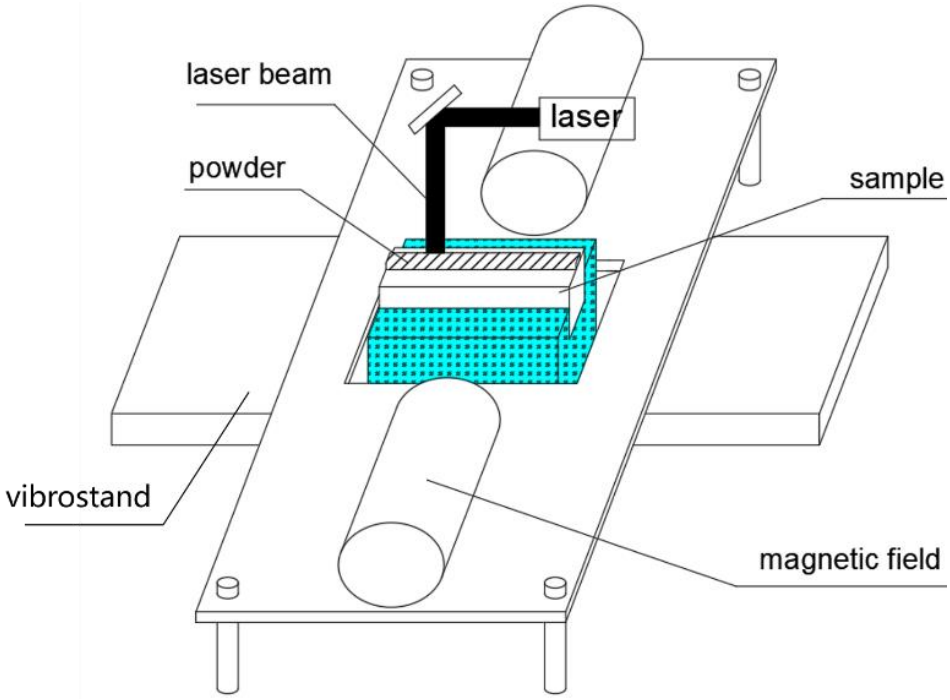


**Figure 1.** Overall structure of coupled field-assisted laser cladding device.

**Table 2.** Comparison table of experimental schemes.

| Sample | 1# | 2# | 3# | 4# |
|---|---|---|---|---|
| Magnetic field intensity (T) | 0 | 0 | 0.8 | 0.8 |
| Amplitude (mm) | 0 | 3 | 0 | 3 |

### *2.2. Characterization*

The phase structure of the coatings was measured by X-ray diffractometer (XRD, Rigaku Corporation, MiniFlex 600, Osaka, Japan) equipped with Cu Kα radiation from 10 to 100° at a scan rate of $10^{\circ}\cdot min^{-1}$. After polishing the sample, corrosion was carried out in aqua regia. The microstructure and chemical composition of the coatings were observed by field emission scanning electron microscope (SEM, Hitachi, SPM-S3400N, Tokyo, Japan). Before observation, samples were polished and then treated by aqua regia ($HNO_3$:HCl = 1:3). The hardness of coatings was tested by a microhardness tester (Yanrun Guangji Technology Co., Ltd., HRS-150, Shanghai, China). The loading and holding time were 1.96 N and 15 s, respectively, and the hardness value was measured by the average value of three points in the same horizontal position. A linear reciprocating wear testing machine (Center for Tribology Inc., UMT-2, Campbell, CA, USA) was used to test the friction and wear properties of the samples at room temperature. During the test, the grinding ball was $Al_2O_3$, and the parameters were controlled at the load of 20 N, the stroke of 5 mm, and the time of 20 min.

## 3. Results and Discussion

### *3.1. Phase Constitution*

The XRD patterns of the coating at different auxiliary fields are demonstrated in Figure 2. It can be confirmed that the phase structure of the Fe60 laser cladding coating is mainly composed of solid solution Ni-Cr-Fe, (Fe, Ni), and Fe-Cr, corresponding to the degree of 44.6°, 64.8°, and 82.1°, respectively. Meanwhile, the coating also contained a certain amount of Cr2Fe14C hard phase. The results indicate that field-assisted laser cladding is able to promote the diffusion of elements in the molten pool and enhance the generation of hard phases.

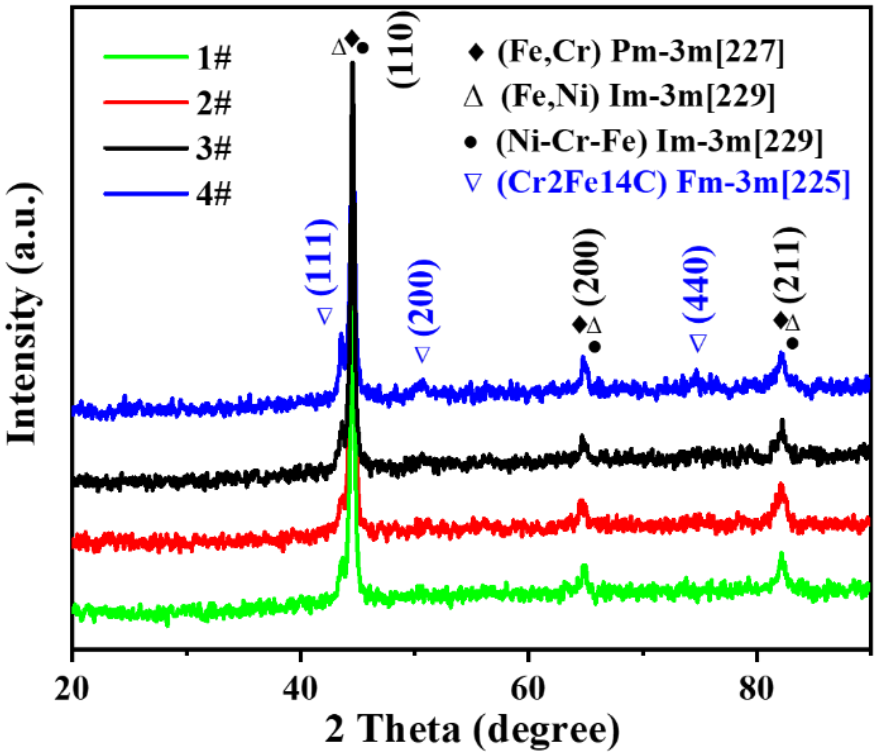


**Figure 2.** XRD patterns of coatings under different field-assisted types.

### *3.2. Microstructure Evolution*

Figure 3 shows the microstructure of the Fe60 laser cladding coating assisted by different fields. The Figure 3a,b shows that the grains of coating are refined, indicating that the large grains are broken into small grains by mechanical vibration field assistance. Interestingly, the grains are also refined in Figure 3c, but the grain arrangement becomes disordered. This can be explained by the circular motion of the flowing metal driven by the Lorentz force induced by steady magnetic field. Under the action of high-energy laser beam irradiation, complex natural convection is exhibited in the melt, and the change of magnetic flux leads to an induced current in the molten pool so that the liquid metal becomes a charged conductor, and the charged liquid metal in the molten pool is bound to be affected by the Lorentz force. Lorentz force in the molten pool also plays a stirring role in the melt in the molten pool, resulting in the grains being refined significantly. Furthermore, under the coupled field-assisted mode with mechanical vibration field and steady magnetic field, the grains are further refined, and the grain arrangement becomes more disordered than the single vibration field assistance.

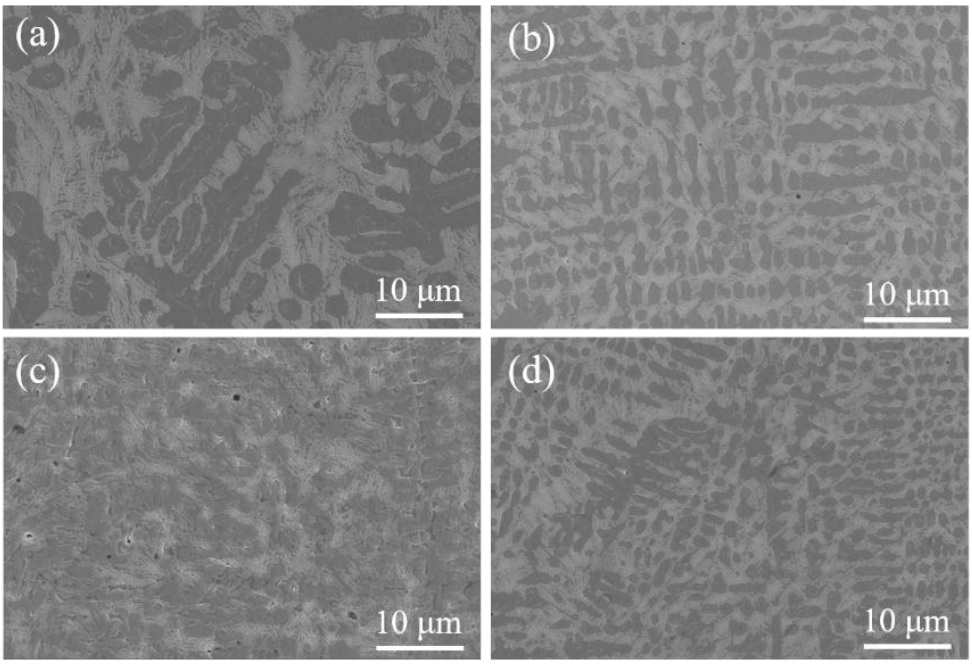


**Figure 3.** The SEM of coatings under different field-assisted types, (**a**) 1#, (**b**) 2#, (**c**) 3#, (**d**) 4#.

The EDS diagram of the coating is shown in Figure 4. Figure 4a is the microstructure of the Fe60 laser cladding coating assisted without field, and Figure 4b is the microstructure of the Fe60 laser cladding coating assisted by coupled field with mechanical vibration field and steady magnetic field. It can be seen that the coatings consist of two parts, the light grey area (ID) and dark grey area (DR). In addition, the elements in the coatings are evenly distributed, indicating that the uniform distribution of coating is promoted by laser cladding. The elemental content calculated by EDS is shown in Table 3. The Cr element content is higher in ID, and meanwhile the contents of C, Fe, and Ni in DR are higher than ID. Importantly, the coating of 4# has the highest C element, which indicates that the content of hard phase is increased. A large amount of hard phase (Cr2Fe14C) is able to enhance the wear resistance of the coating. Therefore, it can be speculated that the coupled field can promote mass transfer in the molten pool to a certain extent, which contributes to the diffusion of Fe, Cr, Ni, and C elements and, thus, promotes the formation of hard phase of Cr2Fe14C.

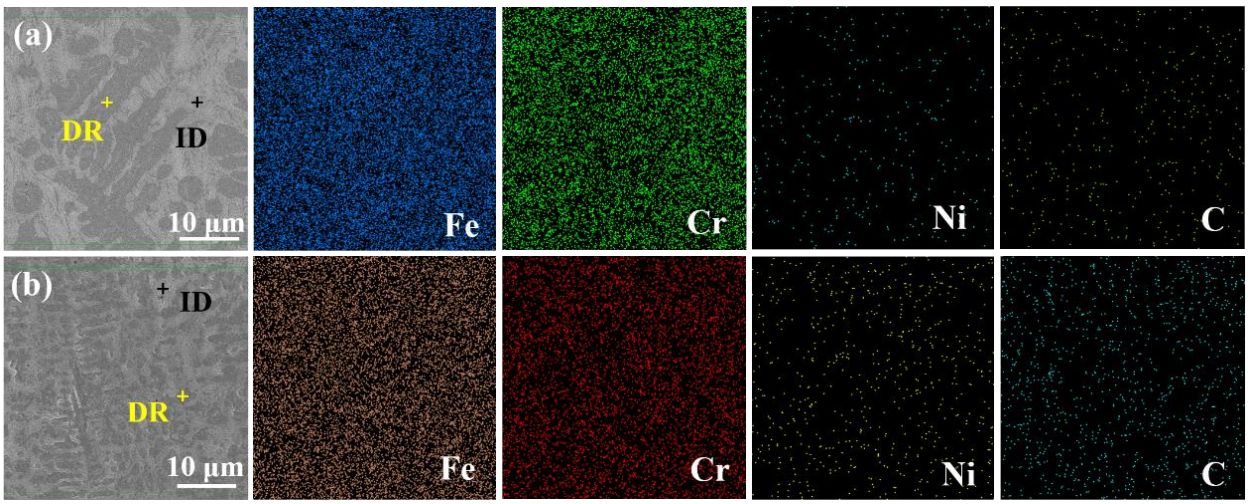


**Figure 4.** EDX of laser cladding coatings of (**a**) 1# and (**b**) 2#.

**Table 3.** EDS analysis results of coatings (at. %).

| Assisted Field | Element | C | Cr | Fe | Ni |
|---|---|---|---|---|---|
| 1# | ID | 15.82 | 17.94 | 55.9 | 0.31 |
| | DR | 23.77 | 11.92 | 56.51 | 0.35 |
| 4# | ID | 23.93 | 15.76 | 47.86 | 0.23 |
| | DR | 26.66 | 10.77 | 53.35 | 0.31 |

### *3.3. Microhardness*

Figure 5 shows the microhardness distribution of the Fe60 laser cladding coating. It can be seen that the hardness of the coating without the field assistance is lower than that of the coating with the field assistance, and the hardness decreases with the increase of the distance from the top of the coating. The maximum hardness of the four samples is 624 $HV_{0.2}$, 653 $HV_{0.2}$, 659 $HV_{0.2}$, and 702 $HV_{0.2}$, respectively. The highest hardness occurs in the laser cladding coating assisted by the coupled field with mechanical vibration field and steady magnetic field. According to the Hall Petch equation [26–28], the hardness of the coating increases as the average grain size decreases.:

$$\sigma_s = \sigma_0 + K_s d^{-1/2} \quad (1)$$

where $\sigma_s$ and $\sigma_0$ are the yield stress and lattice friction stress, $K_s$ is positive constant of yielding associated with the stress required to extend dislocation activity into adjacent unyielded grains, and $d$ is the average diameter of grains.

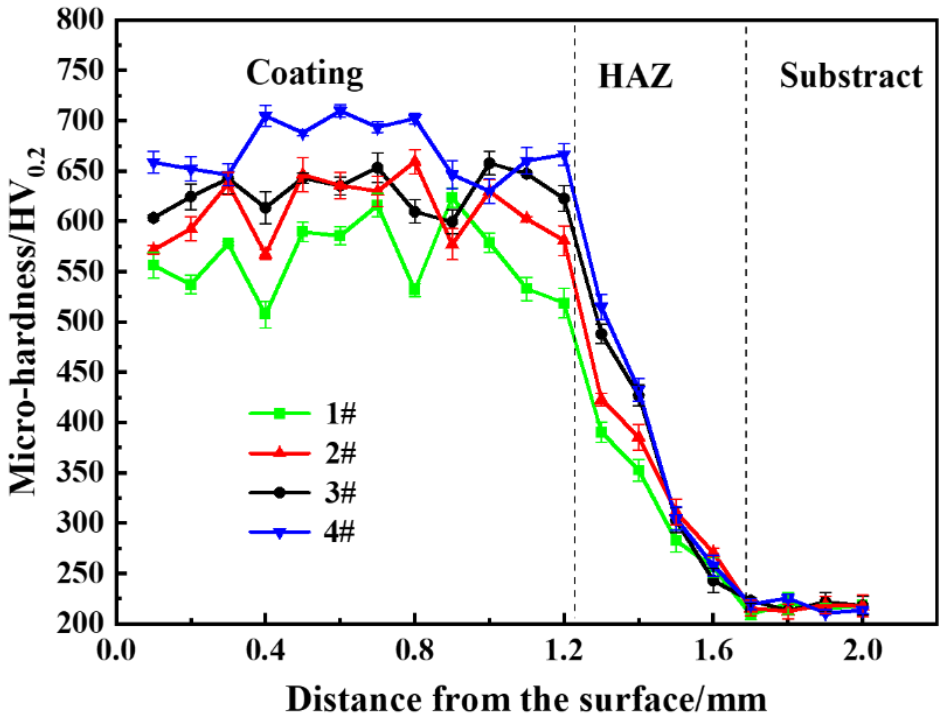


**Figure 5.** Microhardness distribution of the coating along the vertical direction under the action of different field-assisted types.

At the same time, grain refinement increases the grain boundary area, contributing to the strength of coatings that are improved by the hindrance effect on dislocation. Furthermore, the increase in hard phase (Cr2Fe14C) enhances the wear resistance of the coating [14,15].

### *3.4. Friction and Wear*

As an important indicator of wear-resistance performance, the friction coefficients of coatings with the different field-assisted types are demonstrated in Figure 6. The low friction coefficient at the beginning is due to the incomplete contact between the coating and the grinding ball, which results in an inaccurate result [29]. When the contact surface changes from point contact to surface contact, the wear enters a stable stage. It can be observed that after 650 s, the friction coefficient presents a stable trend, and the wear mechanism changes from sharp wear to smooth wear. The coating without field assistance shows a maximum friction coefficient, and the sample of 4# exhibits a minimum friction coefficient. As shown in Figure 6b, the coating wear volume of the 1# is 5950 μm$^3$, while the coating of 4# is 1848 μm$^3$, which reaches the minimum value. The Archard wear equation is an equation derived from a simplified model of abrasive wear, and, although it does not consider the factors such as work hardening and friction heat, it relates the wear rate to engineering variables and mechanical properties of the material. The expression of Archard's wear equation [30] is:

$$\frac{W_v}{S} = K\frac{F}{H} \tag{2}$$

where $W_v$ is the volume wear (μm$^3$), $S$ is the sliding distance (mm), $F$ is the normal load (N), $H$ is the hardness of the wear material (HV), and $K$ is the wear coefficient.

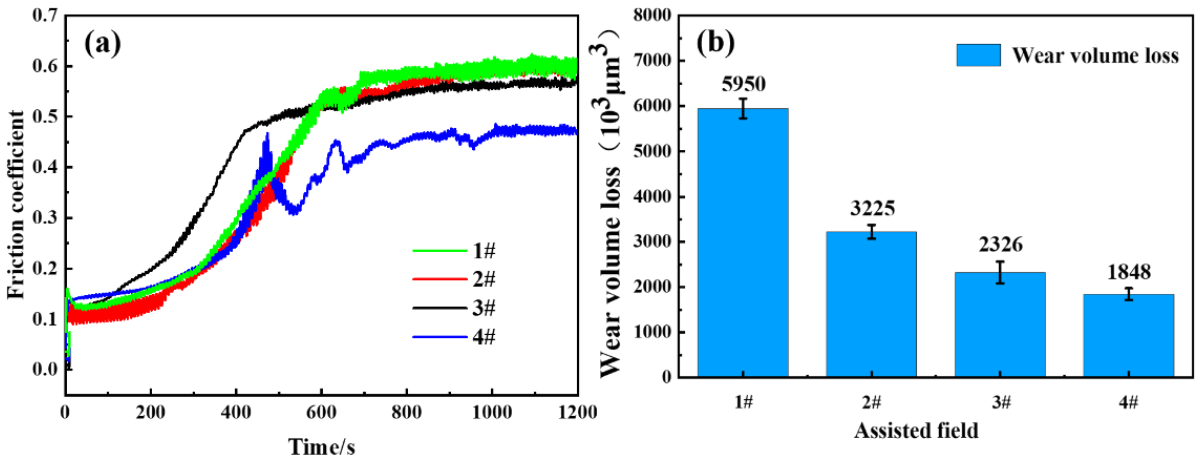


**Figure 6.** The friction properties of cladding coating under different field-assisted types, (**a**) Friction coefficient curve and (**b**) wear volume loss.

According to the microhardness test, it can be concluded that the hardness is inversely proportional to the wear quantity. Therefore, the experimental results are in good agreement with Archard's equation.

Figure 7 is the mechanism diagram of the effect of grains in laser cladding coating caused by different field-assisted types. $F_L$ is Lorentz force; $Fv$ is force generated by vibration field; $G$ is gravity. During the laser cladding process, the thermal convection in the molten pool tungsten is performed by the laser beam, and the movement of molten metal is driven by the thermal convection. The movement of molten metal promotes the mixing of elements in the coating. When the laser cladding process is assisted by the vibration field, the growing dendrites are broken, and the broken nuclei are brought to the melt under the action of vibration and stirring to form a large number of nuclei. Meanwhile, the stirring generated by the vibration also hinders the free growth of dendrites. Therefore, grains are refined. When the laser cladding process is assisted by the steady magnetic field, the Lorentz force causes the metal to be subjected to a vertical and straight inward force, which strengthens the stirring in the direction perpendicular to the flow direction of the liquid. This causes the grain to be arranged in circular trajectories and promotes the refinement of the grains. When the laser cladding process is assisted by the coupled field

with the steady magnetic field and vibration field, the liquid metal in the molten pool is fully stirred; the heat diffusion in the molten pool is accelerated; the temperature gradient in front of the solid–liquid interface decreases; and the large-size dendrites are broken. Furthermore, the grains are further refined and exhibit the same arrangement rule as the grains which are assisted by the magnetic field.

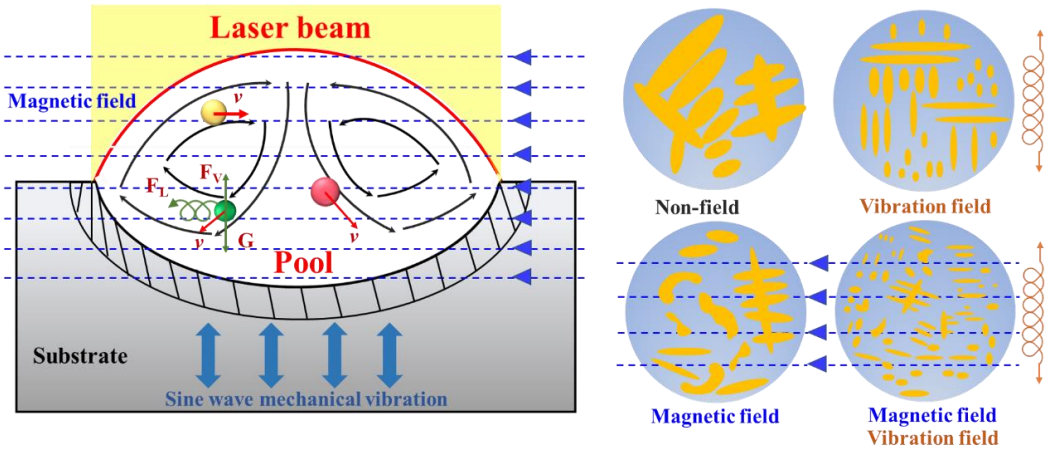


**Figure 7.** The mechanism of the effect of grains in laser cladding coating caused by different field-assisted types.

Figure 8 shows the worn surface morphology of the coating assisted by different fields, which are examined in detail using SEM after being subjected to sliding wear under the same loads. It can be seen from Figure 8a that there are wide and deep grinding furrows on the surface of the abrasion mark without field assistance. In addition, the adhesive wear is present on the coating surface. Importantly, the grinding furrows' width in Figure 8b,c is significantly reduced, and the furrow depth is much smaller than the coating without field assistance. Figure 8d shows the coating wear morphology assisted by the coupled fields of magnetic field and vibration field. Compared with the coating assisted by a single field, the surface grinding furrow is shallower and the wear debris is smaller. Combined with the three-dimensional wear topography (Figures S2 and S3), it can be seen that the coating of 4# has the best abrasion resistance, indicating that the refined grains and the increase in hardness improve the wear resistance of the coating.

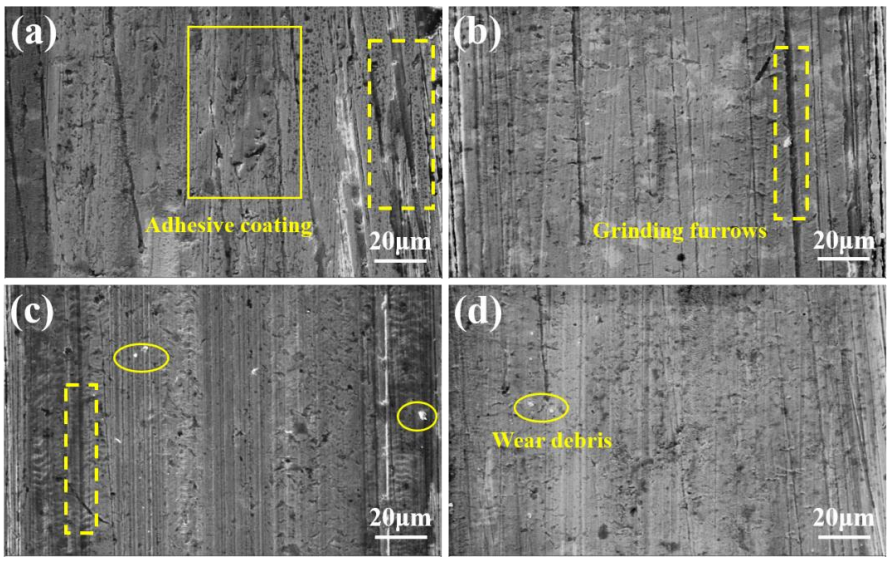


**Figure 8.** The SEM of coatings after linear reciprocating wear testing (**a**) 1#, (**b**) 2#, (**c**) 3#, (**d**) 4#.

## 4. Conclusions

The Fe60 laser cladding coating is prepared on the surface of 45 steel with the assistance of alternating magnetic field–mechanical vibration coupling field. The structure and wear resistance of coatings are investigated.

The structure in the coating is mainly composed of solid solution Ni-Cr-Fe, (Fe, Ni), and Fe-Cr and also contains a certain amount of Cr2Fe14C hard phase. The composition of the coating is not changed by the addition of the assisted field.

When the coating is assisted by the coupled fields, the steady magnetic field and vibration field enhance the stirring effect in the molten pool, and the grains are further refined and exhibit the same arrangement rule as the grains which are assisted by the magnetic field. Meanwhile, the heat diffusion in the molten pool is accelerated by the steady magnetic field; the temperature gradient in front of the solid—liquid interface decreases; and the large-size dendrites are broken. Those contribute to the grains being refined significantly.

The minimum grain size and maximum hard phase content in the coating obtained by the coupled field assistance lead to the maximum microhardness of the coating (702 $HV_{0.2}$) and the minimum wear volume loss (1848 $\mu m \cdot cm^{-3}$). This work broadens the research of the laser cladding coating field and contributes to the development of wear-resistant materials.

**Supplementary Materials:** The following supporting information can be downloaded at: https://www.mdpi.com/article/10.3390/coatings12060751/s1, Figure S1: Self-made magnetic field generation equipment (a) power (b) exciter. Figure S2: 3D morphology of the friction surface with the coating, (a) 1#, (b) 2#, (c) 3#, (d) 4#. Figure S3: The figure of coating wear section (a) 1#, (b) 2#, (c) 3#, (d) 4#.

**Author Contributions:** Conceptualization, Y.W. and H.S.; methodology, Y.W.; validation H.S. and X.H.; formal analysis, H.L. and X.Z.; investigation, Y.W. and H.S.; data curation, Y.W.; writing—original draft preparation Y.W.; writing—review and editing, Y.W.; visualization, H.S.; supervision, H.L.; project administration, H.L. and X.Z.; funding acquisition, H.L. All authors have read and agreed to the published version of the manuscript.

**Funding:** This work was funded by the National Natural Science Foundation of China (No. 61963021).

**Institutional Review Board Statement:** Not applicable.

**Informed Consent Statement:** Not applicable.

**Data Availability Statement:** Data is contained within the article.

**Conflicts of Interest:** The authors declare no conflict of interest

## References

1. Grairia, A.; Beliardouh, N.E.; Zahzouh, M.; Nouveau, C.; Besnard, A. Dry sliding wear investigation on tungsten carbide particles reinforced iron matrix composites. *Mater. Res. Express* **2018**, *5*, 116528. [CrossRef]
2. Shu, D.; Cui, X.; Li, Z.; Sun, J.; Wang, J.; Chen, X.; Dai, S.; Si, W. Effect of the Rare Earth Oxide $CeO_2$ on the Microstructure and Properties of the Nano-WC-Reinforced Ni-Based Composite Coating. *Metals* **2020**, *10*, 383. [CrossRef]
3. Van Acker, K.; Vanhoyweghen, D.; Persoons, R.; Vangrunderbeek, J. Influence of tungsten carbide particle size and distribution on the wear resistance of laser clad WC/Ni coatings. *Wear* **2005**, *258*, 194–202. [CrossRef]
4. Hu, Y.; Wang, L.; Yao, J.; Xia, H.; Li, J.; Liu, R. Effects of electromagnetic compound field on the escape behavior of pores in molten pool during laser cladding. *Surf. Coat. Technol.* **2020**, *383*, 125198. [CrossRef]
5. Barr, C.; Da Sun, S.; Easton, M.; Orchowski, N.; Matthews, N.; Brandt, M. Influence of macrosegregation on solidification cracking in laser clad ultra-high strength steels. *Surf. Coat. Technol.* **2018**, *340*, 126–136. [CrossRef]
6. Liu, J.; Li, J.; Cheng, X.; Wang, H. Effect of dilution and macrosegregation on corrosion resistance of laser clad AerMet100 steel coating on 300M steel substrate. *Surf. Coat. Technol.* **2017**, *325*, 352–359. [CrossRef]
7. Todaro, C.J.; Easton, M.A.; Qiu, D.; Zhang, D.; Bermingham, M.J.; Lui, E.W.; Brandt, M.; StJohn, D.H.; Qian, M. Grain structure control during metal 3D printing by high-intensity ultrasound. *Nat. Commun.* **2020**, *11*, 142. [CrossRef]
8. Farahmand, P.; Liu, S.; Zhang, Z.; Kovacevic, R. Laser cladding assisted by induction heating of Ni–WC composite enhanced by nano-WC and La2O3. *Ceram. Int.* **2014**, *40*, 15421–15438. [CrossRef]

9. Yao, Z.; Yu, X.; Nie, Y.; Lu, X.; Zhang, Q.; Yao, J. Effects of three-dimensional vibration on laser cladding of SS316L alloy. *J. Laser Appl.* **2019**, *31*, 032013. [CrossRef]
10. Zhu, L.; Yang, Z.; Xin, B.; Wang, S.; Meng, G.; Ning, J.; Xue, P. Microstructure and mechanical properties of parts formed by ultrasonic vibration-assisted laser cladding of Inconel 718. *Surf. Coat. Technol.* **2021**, *410*, 126964. [CrossRef]
11. Todaro, C.J.; Easton, M.A.; Qiu, D.; Brandt, M.; St. John, D.H.; Qian, M. Grain refinement of stainless steel in ultrasound-assisted additive manufacturing. *Addit. Manuf.* **2021**, *37*, 101632. [CrossRef]
12. Ma, G.; Yan, S.; Wu, D.; Miao, Q.; Liu, M.; Niu, F. Microstructure evolution and mechanical properties of ultrasonic assisted laser clad yttria stabilized zirconia coating. *Ceram. Int.* **2017**, *43*, 9622–9629. [CrossRef]
13. Wang, H.; Hu, Y.; Ning, F.; Cong, W. Ultrasonic vibration-assisted laser engineered net shaping of Inconel 718 parts: Effects of ultrasonic frequency on microstructural and mechanical properties. *J. Mater. Process. Technol.* **2020**, *276*, 116395. [CrossRef]
14. Ji, X.; Luo, C.; Sun, Y.; Zhao, J. Corrosive wear of multi-layer Fe-based coatings laser cladded from amorphous powders. *Wear* **2019**, *438*, 203113. [CrossRef]
15. Xu, M.; Tang, J.; Ye, N.; Chen, X.; Hu, M. Microstructure and mechanical properties of laser-cladded WC–Co composite coatings on Ti–6Al–4V. *Mater. Res. Express* **2020**, *6*, 1265k2. [CrossRef]
16. Alavi, S.H.; Harimkar, S.P. Melt expulsion during ultrasonic vibration-assisted laser surface processing of austenitic stainless steel. *Ultrasonics* **2015**, *59*, 21–30. [CrossRef]
17. Li, M.; Han, B.; Wang, Y.; Song, L.; Guo, L. Investigation on laser cladding high-hardness nano-ceramic coating assisted by ultrasonic vibration processing. *Optik* **2016**, *127*, 4596–4600. [CrossRef]
18. Zhai, L.L.; Ban, C.Y.; Zhang, J.W. Microstructure, microhardness and corrosion resistance of NiCrBSi coatings under electromagnetic field auxiliary laser cladding. *Surf. Coat. Technol.* **2019**, *358*, 531–538. [CrossRef]
19. Wang, L.; Yao, J.; Hu, Y.; Song, S. Suppression effect of a steady magnetic field on molten pool during laser remelting. *Appl. Surf. Sci.* **2015**, *351*, 794–802. [CrossRef]
20. Liang, W.; Yong, H.; Shiying, S.; Sanpin, L.; Jianhua, Y. Suppression effect of a steady magnetic field on surface undulation during laser remelting. *Chin. J. Lasers* **2015**, *42*, 1103005. [CrossRef]
21. Chen, L.; Yang, Y.; Jiang, F.; Li, C. Experimental investigation and FEM analysis of laser cladding assisted by coupled field of electric and magnetic. *Mater. Res. Express* **2018**, *6*, 016516. [CrossRef]
22. Xie, X.; Zhou, Q.; Chen, L.; Xiao, C.; Tang, X. Microstructure refinement of superalloy K4169 with compound treatment of pulsed magnetic field and mechanical vibration. *Rare Metal Mat. Eng.* **2015**, *44*, 3166–3172.
23. Xie, X.; Zhou, Q.; Chen, L.; Xiao, C.; Tang, X. Effect of compound treatment of pulsed magnetic field and mechanical vibration on grain size and mechanical properties of H62 brass. *Spec. Casting Nonferr. Alloy* **2014**, *34*, 1000–1004.
24. Xie, X.; Zhou, Q.; Chen, L.; Xiao, C.; Tang, X. Effect of compound treatment of pulsed magnetic field and mechanical vibration on solidification structure and hardness of H62 brass. *Foundry* **2014**, *63*, 424–428.
25. Ge, H.; Fang, H.; Zhang, C.; Wang, L.; Zhang, Q.; Yao, J. The evolution of element distribution during laser cladding under static magnetic field. *Metall. Mater. Trans. A* **2022**, *53*, 370–376. [CrossRef]
26. He, J.Y.; Liu, W.H.; Wang, H.; Wu, Y.; Liu, X.J.; Nieh, T.G.; Lu, Z.P. Effects of Al addition on structural evolution and tensile properties of the FeCoNiCrMn high-entropy alloy system. *Acta Mater.* **2014**, *62*, 105–113. [CrossRef]
27. Qin, X.F.; Sun, D.L.; Wang, T.; Zhao, X.G.; Xie, L.Y.; Wu, Q. Hall-Petch and inverse Hall-Petch effects accompany the long-term use of backup roll material. *J. Alloy. Compd.* **2015**, *640*, 497–500. [CrossRef]
28. Sato, Y.S.; Urata, M.; Kokawa, H.; Ikeda, K. Hall-Petch relationship in friction stir welds of equal channel angular-pressed aluminum alloys. *Mat. Sci. Eng. A.* **2003**, *354*, 298–305. [CrossRef]
29. Baek, G.Y.; Shin, G.Y.; Lee, K.Y.; Shim, D.S. Mechanical properties of tool steels with high wear resistance via directed energy deposition. *Metals* **2019**, *9*, 282. [CrossRef]
30. Fu, B.; Feng, K.; Li, Z. Study on the effect of Cu addition on the microstructure and properties of NiTi alloy fabricated by laser cladding. *Mater. Lett.* **2018**, *220*, 148–151. [CrossRef]